EFDA–JET–PR(11)32

E. Lerche, D. Van Eester, J. Ongena, M.-L. Mayoral, M. Laxaback, F. Rimini, A. Argouarch, P. Beaumont, T. Blackman, V. Bobkov, D. Brennan, A. Brett, G. Calabro, M. Cecconello, I. Coffey, L. Colas, A. Coyne, K. Crombe, A. Czarnecka, R Dumont, F. Durodie, R. Felton, D. Frigione, M. Gatu Johnson, C. Giroud, G. Gorini, M. Graham, C. Hellesen, T. Hellsten, S. Huygen, P. Jacquet, T. Johnson, V. Kiptily, S. Knipe, A. Krasilnikov, P. Lamalle, M. Lennholm, A. Loarte, R. Maggiora, M. Maslov, A. Messiaen, D. Milanesio, I. Monakhov, M. Nightingale, C. Noble, M. Nocente, L. Pangioni, I. Proverbio, C. Sozzi, M. Stamp, W. Studholme, M. Tardocchi, T.W. Versloot, V. Vdovin, M. Vrancken, A. Whitehurst, E. Wooldridge, V. Zoita and JET EFDA contributors

Optimizing ICRF Heating for ITER: Dedicated JET Experiments

Optimizing ICRF Heating for ITER: Dedicated JET Experiments

E. Lerche[1], D. Van Eester[1], J. Ongena[1], M.-L. Mayoral[2], M. Laxaback[3], F. Rimini[2], A. Argouarch[4], P. Beaumont[2], T. Blackman[2], V. Bobkov[5], D. Brennan[2], A. Brett[2], G. Calabro[6], M. Cecconello[7], I. Coffey[2], L. Colas[4], A. Coyne[2], K. Crombe[8], A. Czarnecka[9], R Dumont[4], F. Durodie[1], R. Felton[2], D. Frigione[6], M. Gatu Johnson[7], C. Giroud[2], G. Gorini[10], M. Graham[2], C. Hellesen[7], T. Hellsten[3], S. Huygen[1], P. Jacquet[2], T. Johnson[3], V. Kiptily[2], S. Knipe[2], A. Krasilnikov[11], P. Lamalle[12], M. Lennholm[2], A. Loarte[12], R. Maggiora[13], M. Maslov[14], A. Messiaen[1], D. Milanesio[13], I. Monakhov[2], M. Nightingale[2], C. Noble[2], M. Nocente[10], L. Pangioni[2], I. Proverbio[10], C. Sozzi[10], M. Stamp[2], W. Studholme[2], M. Tardocchi[10], T.W. Versloot[15], V. Vdovin[16], M. Vrancken[1], A. Whitehurst[2], E. Wooldridge[2], V. Zoita[17]
and JET EFDA contributors

JET-EFDA, Culham Science Centre, OX14 3DB, Abingdon, UK

[1]LPP-ERM/KMS, Association Euratom-'Belgian State', TEC Partner, Brussels, Belgium
[2]EURATOM-CCFE Fusion Association, Culham Science Centre, OX14 3DB, Abingdon, OXON, UK
[3]Fusion Plasma Physics, Association Euratom-VR, KTH, Stockholm, Sweden
[4]CEA (IRFM)-Euratom Association, Saint-Paul-lez-Durance, France
[5]IPP (MPI)-Euratom Association, Garching, Germany
[6]C. R. Frascati, Euratom-ENEA sulla Fusione, Frascati, Italy
[7]Uppsala University, Association EURATOM-VR, Uppsala, Sweden
[8]Department of Applied Physics, Ghent University, B-9000 Ghent, Belgium
[9]Institute of Plasma Physics and Laser Microfusion, Warsaw, Poland
[10]Instituto di Fisica del Plasma, EURATOM-ENEA-CNR Association, Milan, Italy
[11]SRC RF Troitsk Institute for Innovating and Fusion Research, Troitsk, Russia
[12]ITER Organization, Saint-Paul-lez-Durance, France
[13]Politecnico di Torino, Euratom-ENEA sulla Fusione, Torino, Italy
[14]CRPP-EPFL, Association Euratom-Confédération Suisse, CH-1015 Lausanne, Switzerland
[15]FOM Institute Rijnhuizen, Association EURATOM-FOM, Nieuwegein, the Netherlands
[16]RNC Kurchatov Institute, Nuclear Fusion Institute, Moscow, Russia
[17]National Institute for Plasma Physics, Association EURATOM-MEdC, Bucharest, Romania
** See annex of F. Romanelli et al, "Overview of JET Results",*
(23rd IAEA Fusion Energy Conference, Daejon, Republic of Korea (2010)).

Preprint of Paper to be submitted for publication in
Plasma Physics and Controlled Fusion

ABSTRACT.
In the past years, one of the focal points of the JET experimental program was on Ion Cyclotron Resonance Heating (ICRH) studies in view of the design and the exploitation of the ICRH system being developed for ITER. In this brief review, some of the main achievements obtained in JET in this field during the last 5 years will be summarized. The results reported here include important aspects of a more engineering nature, such as (i) the appropriate design of the RF feeding circuits for optimal load resilient operation and (ii) the test of a compact high power density antenna array, as well as RF physics oriented studies aiming in refining the numerical models used for predicting the performance of the ICRH system in ITER. The latter include (i) experiments designed for improving the modelling of the antenna coupling resistance in various plasma conditions and (ii) the assessment of the heating performance of ICRH scenarios to be used in the non-active operation phase of ITER.

1. INTRODUCTION

Ion Cyclotron Resonance Frequency (ICRF) heating is one of the main auxiliary heating systems foreseen for ITER [1, 2]. Together with neutral beam injection NBI (33MW) and electron cyclotron resonance heating ECRH (20MW), it is expected to provide 20MW of heating power to help the ITER plasmas achieving fusion relevant temperatures. Because most of the ICRF power applied is typically absorbed by the ions, this heating method is expected to have the strongest impact on the DT fusion yield per MW of external power applied to the plasma.
The basic principles of ICRF heating are illustrated in Fig.1:

(1) A high power Radio-Frequency (RF) generator is connected by a long transmission line to poloidal strap antennas located inside the vacuum vessel of the tokamak. A matching circuit (composed by transmission line elements of variable length) is used to assure real-time impedance matching between the high Z generator and the antenna array during a plasma discharge.
(2) The antenna excites fast wave modes that are evanescent in the low density region of the Scrape-Off Layer (SOL) but become propagative near the plasma separatrix, where the plasma density becomes larger.
(3) The fast wave modes propagate towards the plasma centre until they reach the cyclotron layer of a given ion species (for which the wave frequency ω is equal to the local ion cyclotron frequency $\omega_{ci} = q_i/m_i \times B_0$), where it is strongly damped by transferring its energy to the resonant ions which are thereby accelerated to supra-thermal energies. These fast ions transfer the absorbed wave energy to the bulk plasma species via collisions (slowing-down) resulting in efficient plasma heating.

For the full process to be efficient, each of the above mentioned steps have to be optimally accomplished:

(1) The generated RF power has to be properly transferred to the antenna, which depends on the

antenna design and on the layout of the impedance matching circuit, which should be capable of maintaining the power reflected from the antenna below a certain level independent of the value of the antenna loading resistance. The quality of the impedance matching is usually expressed in terms of the voltage standing wave ratio VSWR = $(|V_{FOR}|+|V_{REF}|) / (|V_{FOR}|-|V_{REF}|)$, where V_{FOR} and V_{REF} are respectively the forward and reflected voltages measured by directional couplers installed in the feeding transmission line.

(2) The power launched by the antenna has to be efficiently coupled to the plasma, what also depends on the antenna design but is particularly sensitive to the characteristics of the plasma in the Scrape-Off Layer (SOL). The efficiency of this process is described by the antenna coupling resistance R_{ant}, which is proportional to the Poynting flux of the RF fields excited and thus describes the amount of RF power that tunnels through the evanescence region and reaches the plasma for a given voltage V applied to the antenna, $P_{RF} \propto R_{ant} \times V2$.

(3) The coupled RF power has to be efficiently absorbed in the plasma, what again depends on the antenna excitation but also depends on the plasma core parameters (n_e, T_e, plasma composition) and on the equilibrium magnetic field B_0. The figure of merit of this process is the heating efficiency $\eta = P_{abs}/P_{RF}$, which quantifies the amount of power that is truly absorbed in the plasma (P_{abs}), as opposed to the power lost by edge processes and ICRF induced radiation losses.

It is clear that maximizing the performance of each of the above described steps is a big challenge, particularly for ITER where, on top of the several design and engineering constraints, ICRF is supposed to reliably deliver a significant amount of power in the different operation phases and in different heating scenarios, despite the unfavourable conditions of the SOL (large antenna plasma distances, strong ELM's).

This work summarizes the latest contributions of the JET experimental program for enhanced ICRF operation in various conditions, aiming at optimizing the design and the operation of the ICRF system for ITER. The paper is divided as follows: Section 2 describes the modifications done in the matching circuit layout of the JET A2 antennas in order to allow efficient RF power coupling during the fast antenna loading variations caused by Edge Localized Modes (ELM's). Section 3 summarizes the key results obtained with the 'ITER-like' Antenna (ILA), a new compact antenna array installed in JET with the objective of testing key features of the ITER antenna design; In section 4, the results of experiments designed to validate RF modelling tools and in particular coupling resistance calculations will be shown, including a review of the estimated coupling expected in ITER. In section 5, the results of some ICRF scenarios proposed for the non-active operation phase of ITER that were recently tested in JET will be summarized and preliminary predictions of their performance in ITER will be drawn. The paper ends with a brief summary and some plans for future investigations.

2. ELM RESILIENT OPERATION OF THE JET A2 ANTENNAS

An ICRH system for ITER and fusion reactor applications has to be able to cope with fast antenna

load variations, such as those produced by ELM's or by pellet injection. In the A2 antenna system in JET [3], consisting of 4 antenna modules each composed by 4 straps fed individually by one amplifier, the impedance matching is achieved with the use mechanical transmission line elements (stubs, trombones), which are too slow to follow the fast (order ~10-50μs) antenna load variations induced by ELM's. This leads to large amounts of reflected power returning to the amplifier, which, to protect itself, shuts down for a certain interval of time. The average power delivered to the plasma is therefore much less than the requested one, with minimal plasma heating as a result.

To demonstrate a solution to this problem two different load resilience concepts have been implemented and tested at JET with the A2 antennas:

(i) A 3dB hybrid matching circuit [4]: Such a system is based on inductively connecting pairs of straps with 3dB hybrid couplers and thereby diverting the reflected power occurring during loading transients to a dummy load (see Fig.2a). This approach was first proven on ASDEX-Upgrade [5]. It provides safe operational conditions for the RF generators at the expense of wasting a fraction of the generated power during ELM's to the dummy load. This system is currently installed on two of the four A2 antenna modules (antennas A and B) and allowed trip-free ICRF operation during most types of ELM's, with time-averaged power levels delivered to H-mode plasmas up to three times larger than was previously possible.

(ii) The Conjugate-T concept (CT), involving pairs of straps connected in parallel to form so called Resonant Double Loops (RDL's) [6]. The two straps in each RDL are fed from a common transmission line via a T-junction, with adjustable matching elements (phase shifters) located between the antenna straps and the conjugate T-point (see Fig.2b). Tolerance to plasma load variations is achieved by adjusting the impedances of the two branches to be complex conjugate. Ideally this results in a purely resistive load seen by the amplifier and as long as the load variations experienced by the two antenna straps are similar, the reflected power keeps being transferred from one antenna branch to the other (within the RDL circuit) resulting in low reflected power levels in the circuit behind the conjugate T-point independent of the value of the loading resistance of the antenna. Such a system with line stretchers (external to the tokamak) as adjusting impedance elements is installed on antennas C and D [7] and also demonstrated good reliability for ICRF operation during strong ELM's. This approach has the advantage that the RF power is also coupled to the plasma during the ELM's (rather than being deviated to an external dummy load) but requires careful tuning of the individual antenna branches for achieving wide load tolerance in different plasma conditions, as opposite to the 3dB concept which is based on a simpler matching principle.

Both the 3dB and the conjugate-T configurations installed in the A2 antenna system proved good RF power coupling reliability in ELMy H-mode plasmas. A second ELM resilient system based on the conjugate-T principle is installed at JET on the 'ITER-Like' Antenna (ILA), as will be described in the next section. Together with the ILA, the ICRF system coupled more than 8MW in strong

type-I ELMy H-mode discharges in JET [8]. An example of one of these pulses is given in Fig.3, where the time traces of the ICRF power coupled by each of the load resilient systems (a) is shown together with the D_α-emission signal (b).

3. KEY RESULTS OF THE JET ITER-LIKE ANTENNA

The concept of high power compact ICRF antennas was put to test with the installation in 2008 of the ITER-Like Antenna (ILA), a compact antenna array ($0.9m^2$) composed of 8 poloidal straps [9, 10]. Each pair of straps is connected in the conjugate-T configuration for extended load tolerance and the individual branch reactance's are tuned with internal matching capacitors. Aside from ELM resilience, this antenna has been specially designed to test key specifications of the ICRF antenna proposed for ITER, requiring reliable operation at high strap voltages and at high power densities with real-time matching of the full compact antenna array, in which the neighbouring straps are strongly coupled to each other.

In figure 4 (left), an example of a high RF power density pulse is given. After the application of 4.3MW of ICRF power (~$5MW/m^2$), the electron temperature increases by 3−4keV illustrating the fact that efficient plasma heating is taking place and that RF-induced radiation losses are small. The monster sawteeth oscillations [11] observed in the T_e signal further corroborate the efficient H minority ion acceleration in the plasma core. Also note that in this case, which features high coupling resistance, the strap voltages are only about 30kV and there is an almost perfect voltage balance on the several antenna straps (c). In similar pulses, a maximum power density of $6.2MW/m^2$ was achieved, which corresponds to the ballpark of the values currently specified for ITER ($6-7MW/m^2$). In figure 4 (right), an example of high voltage operation with the lower half of the ILA antenna is given. Because this is a H-mode discharge, the coupling resistance is relatively low and for coupling about 2MW of RF power with half of the antenna it was necessary to increase the antenna voltages to ~40kV. Also note that the strap voltages are somewhat less balanced than in the L-mode discharge (left), a consequence of the enhanced influence of the mutual coupling between straps on the antenna control when the coupling resistance is low [12]. The maximum voltage achieved in arc-free ILA operation was about 43kV, a value that again meets the requirements proposed for the ITER antenna (V<45kV).

The good performance of the ILA antenna in JET together with extensive RF modelling of the experimental results increased our confidence on key aspects of the ITER antenna design, in particular on the capability of operating compact antennas with high power densities and at high strap voltages. Unfortunately, due to a technical failure of one of the matching capacitors, only half of the antenna array remained operational during most part of the H-mode commissioning phase and other important milestones, such as demonstrating full power capabilities in ELMy H-mode plasmas couldn't be achieved.

4. ANTENNA COUPLING STUDIES

As mentioned, the coupling resistance (or loading resistance) of the antenna is proportional to the Poynting flux associated to the RF fields near the plasma edge and therefore 'dictates' the RF power that can be coupled to the plasma for a given voltage or current in the antenna straps. This quantity not only depends on several RF parameters, such as the wave frequency and the $k_{//}$ spectrum excited by the antenna, but is particularly sensitive to the properties of the scrape-off layer and the plasma edge. To illustrate the parametric dependence of the coupling resistance with a few key quantities and to benchmark the numerical modelling tools used for designing the ITER ICRF antenna, a series of experiments were carried out in which the antenna-plasma distance was scanned during each pulse while the loading resistance was monitored, as illustrated in Fig.5 (left). In Fig.5 (right), the coupling resistance of one pair of the ILA straps is plotted against the antenna-plasma distance for an L-mode discharge at f = 42MHz. As expected, the resistance decreases exponentially with the antenna-plasma distance [13] and it varies by a factor of ~2 when the plasma is shifted away from the antenna by only 4cm. The modelling done with the TOPICA code [14] confirms this behaviour and is in very good agreement with the experimental data. The large errorbars associated to the numerical predictions are a consequence of the uncertainties in the RF measurements and in particular on the edge density measurements (exact location of the cut-off position).

In figure 6 (left), the coupling resistances obtained in two similar L-mode discharges operating at 42MHz and 33MHz are compared. It is clear that the coupling resistance values (and thus the power capabilities) are strongly reduced when operating at lower frequencies, because these waves are more evanescent than the high frequency waves in the SOL leading to smaller RF fields at the plasma edge for the same voltage imposed in the antenna. Figure 6 (right) illustrates the effect of the density gradient in the plasma edge on the antenna loading, where the reference L-mode discharge at f = 42MHz shown in (b) is compared with an H-mode discharge with the same RF operating frequency. One sees that the coupling resistance is reduced for the case of the H-mode discharge and that this reduction is even stronger when the antenna-plasma distance is smaller. The main reason for the R_{ant} decrease in H-mode is not the change in the SOL density values but rather the steeper density gradients that exist in the plasma edge (inside the propagative region of the waves) in the H-mode discharges, which are characterized by a higher pedestal density. This effect is called *refractive index mismatch* and is related to the higher wave reflection in the case of steep refractive index (density) gradients [15].

In a different series of experiments done with the A2 antennas, the influence of the antenna phasing on the coupling resistance was investigated. In figure 7 the average coupling resistances of the antenna modules A and B are plotted as function of the dominant $k_{//}$ wavenumber excited in each of the different antenna phasings adopted. In figure 7 (right) the corresponding $k_{//}$-spectra excited in three phasing configurations computed with the ANTITER II code [16] are illustrated: $0\pi0\pi$ (solid), $0\pi\pi0$ (dashed), $00\pi\pi$ (dash-dotted). All the pulses were done at $B_0 = 3.0T$ / $I_P = 2MA$ with an RF frequency of f = 42MHz and a fixed antenna-plasma distance of d = 0.11m. The dashed curve on the

left figure illustrates the approximate exponential dependence of the coupling resistance with the dominant $k_{//}$ wavenumber excited. Note that by operating at e.g. $00\pi\pi$, the coupling resistance can be improved by ca. 30% with respect to the standard dipole configuration ($0\pi0\pi$) typically used.

In this same experimental campaign, the ICRF heating efficiency as well as the RF-induced plasma-wall interaction was also studied. It was observed that, for the T = 5keV target plasmas adopted in these experiments, operating at antenna phasings with dominant $k_{//}$ values lower than $4m^{-1}$ caused a strong degradation in the heating performance [17]. The decrease in the plasma absorptivity at low $k_{//}$ has been corroborated numerically by 1D wave calculations done with the TOMCAT code [18] and is related to the narrower ion-cyclotron absorption region obtained at low $k_{//}$ for a given plasma temperature. Preliminary predictions indicate that this deleterious effect will be negligible in ITER even when operating at the lowest $k_{//}$ phasing foreseen ($00\pi\pi$), as long as the plasma temperature is sufficiently high (T > 8-10keV). Another important outcome of these experiments was the enhanced plasma-wall interaction observed at low $k_{//}$ phasing configurations, leading to a higher plasma impurity content and therefore higher RF-induced radiation losses [19, 20]. These observations are consistent with enhanced RF sheath rectification effects, i.e. to the fact that the parallel RF electric field excited close to the antenna is larger for the low $k_{//}$ phasing configurations (where neighbouring pairs of straps are fed with currents of equal phase) and non-resonant acceleration of charged particles in the SOL is enhanced [21]. Numerical modelling of these experiments using the HFSS code confirms that the near fields and the image currents excited in the antenna box are indeed expected to be larger in the low $k_{//}$ cases [22].

As mentioned before, the value of the plasma density in the SOL and in the vicinity of the cut-off density region also has a strong influence on the coupling resistance. Experiments aiming at enhancing the antenna loading by injecting small amount of gas from different locations in the tokamak in conditions similar to the ones expected in ITER have been carried out on JET and on other machines [23, 24]. Although gas injection from divertor, top or midplane led to a global modification of the SOL density profiles significant enough to improve the ICRF coupling, it was also shown that an injection near the antennas could lead to an additional ICRF coupling improvement for the same amount of gas injected. As expected, gas injection was found to affect (differently depending on the plasma configuration pumping and recycling properties) the plasma pedestal and hence the bulk plasma confinement properties but so far, the disadvantages associated with such a decrease compared to the advantages of a potential increase in the power input to the plasmas centre was not investigated nor quantified [23].

The strong sensitivity to the SOL properties is further reflected in the numerical predictions of the power capabilities of the ITER ICRF antennas. Recent studies have shown that the expected coupling resistance can change by a factor of roughly 6 when considering the most optimistic and the most pessimistic SOL density profiles currently computed for ITER [16]. Even in the worst case scenario (in which the density is so low that one could claim that the plasma can safely be shifted closer to the antenna to enhance the coupling) the power coupled per antenna module is about 12MW, still

above the minimum specifications of the ITER antenna design (10MW). In the same study it was also shown that, by operating at the standard dipole antenna phasing configuration ($0\pi0\pi$) instead of operating with the reference phasing $0\pi\pi0$, the coupling resistance can be degraded by a factor of two. Efforts trying to reduce the uncertainties on the ICRF power capability predictions for ITER based on adopting different SOL profiles which nevertheless feature similar heat-loads in the first wall (rather than similar antenna-plasma distances) are ongoing.

5. DEVELOPMENT OF ICRF HEATING SCHEMES FOR ITER'S NON-ACTIVE PHASE

Prior to the main phase of exploitation to be performed at the full magnetic field of 5.3T with deuterium - tritium plasmas [25, 26], the ITER tokamak will first go through a commissioning phase at half of its nominal magnetic field ($B_0 = 2.65$T). This phase is intended to test the plasma behaviour and its main properties while the full heating becomes available and to test the diagnostics in a less harsh environment than that of a burning plasma. To avoid premature activation of the machine, hydrogen (H) and/or helium (^{4}He) rather than deuterium (D) and tritium (T) will be adopted as a majority gas during that initial phase.

In the foreseen frequency range of the ITER ICRF system (f = 40-55MHz) the following two heating scenarios are possible for the ITER non activated phase at half-field:

(i) Hydrogen heating at its fundamental (N = 1) cyclotron resonance around f = 42MHz (see Fig.8a), either in pure H plasmas or in ^{4}He plasmas. While the latter (known as H minority ICRF heating) is commonly used in present-day tokamaks due to its high heating efficiency [27], the ion-cyclotron heating of single ion species plasmas is known to be less efficient and therefore has not been as much explored in current day machines.

(ii) ^{3}He heating at its second harmonic (N = 2) cyclotron resonance around f = 53MHz in H or ^{4}He plasmas (see Fig.8b). In view of the sizeable volume of ITER and the cost of this Helium isotope, large ^{3}He concentrations will however be avoided in this next step machine. This compromises the efficiency of this heating scenario, as will be shown later. Note that this scheme is a mock-up of the heating scheme foreseen for the machine's activated DT phase: as the charge-to-mass ratio (Z/A) of D and T are half of the ratio for H and ^{3}He, the respective cyclotron layers in H-$_3$He plasmas at half field are at the same positions as the D-T cyclotron layers at ITER's full field, $B_0 = 5.3$T (see Fig.8c). Therefore, the local wave dispersion and thus the RF field structure will be similar in both cases.

In preparation for ITER's half-field operation phase, and as the JET A2 frequency range allows it, a set of experiments were conducted in H plasmas to test the two heating schemes just described [28]. The RF frequency used was f = 42MHz for the fundamental H majority heating experiments and f = 52MHz for the N = 2 ^{3}He ones. Dipole phasing was adopted and up to $P_{RF} = 5.5$MW was coupled to the plasma. The central density was around $3.0\text{-}3.5\times10^{19}$m^{-3}, which is comparable to the density expected in the initial operation of ITER. Central ion and electron temperatures of 2-3keV were

reached, which are well below the expected temperatures of the initial ITER plasmas (8-10keV).

Figure 9 (left) depicts the measured (symbols) and calculated (lines) heating efficiencies for the H majority heating scenario as function of the plasma temperature. The experimental data was obtained by modulating the RF power and studying the ion and electron temperature responses by break-in-slope analysis techniques [29]. JET is equipped with diagnostics that allow pinning down the temperature profiles with sufficient spatial and temporal resolution to yield meaningful results about where the externally launched waves transfer their energy to the plasma. The ion temperature profile is obtained via charge exchange diagnostics [30], while the electron temperature profile is estimated from electron cyclotron emission measurements [31].

One can clearly see that the electron absorption (~20%) systematically dominates the ion absorption (~15%) and that the total heating efficiency slightly increases with the plasma temperature from 30-40% in the studied interval. These low values indicate that this is not a particularly efficient heating scheme (a typical figure of merit for hydrogen minority heating in D plasmas – the most widely used RF heating scheme in JET - is around 80-90%). A non-negligible fraction of the power is lost through RF-induced radiation (~30%), and the scaling of the impurity content with the RF power suggests that there is significant interaction of the edge electric fields with the wall. Note that up to a point, optimizing the antenna structure allows reducing the sheath effects near the antenna but the large electric fields set up at the plasma edge and in the scrape-off layer are hard to avoid in schemes characterized by low single pass absorption. The importance of taking into account the RF power losses in low absorption scenarios can readily be seen when comparing the theoretical single pass absorption predictions obtained by the 1D wave code TOMCAT [18] (grey curves in figure 9-left) with the experimental findings: although the single pass absorption values confirm the relative importance of ion versus electron heating, the summed absorption is too low (~10%). When realizing that the power is sloshing through the machine a number of times before being fully absorbed by the plasma, it becomes clear that a model that includes the edge losses per single pass of the ICRF waves in the plasma is needed to simulate the experimental heating efficiencies found. As shown in figure 9 (left), good agreement between the experimental values and the multi-pass absorption predicted by TOMCAT is obtained when *single pass losses* of 22% are considered in the multi-pass model, a value that is twice as large as the single pass absorption (~10-12%)

When examining the same scenario for ITER (Fig.9 - right), similar conclusions as for JET can be drawn, although the size of the machine and the higher temperatures yield somewhat less pessimistic single pass absorption figures: at the temperature projected to be reached in the L-mode ITER phase (8-10keV) the ions absorb 7% of the power while the electrons absorb 18% in a single transit over the plasma, yielding a global single pass absorption in the range of 25% (grey curves). Assuming that the losses will be similar in the edge of the ITER machine as those found for JET, the projected overall heating efficiency is in the range of 50-60% in the temperature range expected in ITER. The fact that the obtained figure sensitively depends on the plasma temperature underlines the need for self-consistent modelling of the heating and transport, a topic outside the scope of the

present paper. Aside from more in depth theoretical analysis to optimize the performance of this ICRF scenario, further experimental study can help to improve this heating scheme in preparation for ITER. Theoretical and experimental evidence suggests that, provided efficient means of preheating the plasma are available, this scheme's efficiency may be increased. Another modestly promising option that has been identified is the change of the gas mixture (e.g. dilution with ^{4}He) to profit from the beneficial role of the change of the RF wave polarization on the heating efficiency.

Except for the different RF frequency and the presence of ^{3}He in the discharges, the plasma parameters for the second harmonic ^{3}He ICRF experiments were the same as those used for the fundamental H heating experiments. The ^{3}He content was scanned from X[^{3}He] = 2% to 25% and was controlled in real-time by an algorithm that estimates the amount of ^{3}He present in the discharge based on edge spectroscopy measurements [32]. Similar to the above discussed H majority case, this scenario proved to be a heating scheme of modest potential, in particular at the low ^{3}He concentration levels relevant for ITER.

This is illustrated in figure 10 (left), where the heating efficiencies obtained in the experiments (symbols) are plotted as function of the ^{3}He concentration in the plasma together with the theoretical predictions (lines). A distinct difference was observed between the electron and ion temperature responses to the modulated RF power (not shown here): while the T_e signal showed a small but clear response to the RF power changes at any ^{3}He concentration level, the ion temperature only started to be modulated at higher ^{3}He concentrations, suggesting that the ion absorption was increased in this regime. The ion response became stronger than the electron one when X[^{3}He] exceeded 20%. This is consistent with the total heating efficiency changes from about 20% to 40% seen in figure 10-left when increasing the ^{3}He concentration from 5% to 25%. This increase is seen to be solely due to the ion heating gradually becoming more efficient with increasing ^{3}He concentration, the electron heating essentially being unaffected. For the N = 2 ^{3}He heating scenario, the dependence of the heating efficiency with the temperature was minor, at least in the limited temperature domain experimentally scanned. As in the H majority heating scheme the theoretical response mimics the experimental data: the electron absorption is unaffected by the change of the minority concentration while the ion heating gradually improves, a characteristic that is typical for second harmonic heating. In agreement with the experiments, numerical absorption estimates show that the electron and ion heating are equally important when X[^{3}He]≈20%. To align the single pass absorption (grey curves) with the experimental heating efficiency (symbols), a 26% single pass loss was assumed in the multi-pass absorption model, a somewhat higher value than obtained for the H majority ICRH case. This is consistent with the higher fraction of RF-induced radiation losses observed in the N = 2 ^{3}He ICRH experiments compared to the N = 1 H majority heating case in spite of the similar heating efficiencies: a 4MW modulation in power yields a 2MW amplitude response of the radiated power, i.e., about half of the coupled RF power is never used to heat the plasma but is lost through enhancement of the radiation processes

When running the simulations for this second heating scheme for the half-field ITER parameters

(see figure 10-right), it can be observed that qualitatively the same trend as observed in JET is to be expected, and that the single pass absorption (grey curves) will be modest (~25%) at the low ^{3}He concentrations being considered for ITER. Although this scheme would become much more efficient at higher ^{3}He concentrations, the amounts of ^{3}He that would be required for such operation are prohibitive. Hence – similar to the previously discussed scheme - a projected heating efficiency of ~50% is foreseen for the ITER baseline conditions when adopting similar losses as the ones found for the JET experiments in the multi-pass absorption model.

Despite the low efficiency of this heating scenario, fast ^{3}He ions up to 200keV were detected by the Neutral Particle Analyser (NPA) diagnostics when 5MW of RF power was applied. Although N = 2 ^{3}He heating was the intended scheme, a fraction of the launched power was also absorbed by fast D ions coming from neutral beam injection at their 3rd harmonic ion cyclotron resonance layer, that lies in between the antenna and the centrally located N = 2 ^{3}He ion cyclotron resonance (see Fig.8b). Since Hydrogen beams were not available, D beams were used both for preheating the plasma and for obtaining the ion temperature from the charge exchange diagnostic. There was evidence that these particles were absorbing a non-negligible part of the RF power: the fast ions detected by the neutral particle analyzer have energies that are a factor 2-3 times beyond the beam source energy (80-130keV) and the fast ion losses (measured with a scintillator probe) were strongly enhanced when D beams and ICRF were simultaneously applied to the plasma [33]. Note that no evidence of RF heated D particles was found in the fundamental H majority heating experiments although the 2nd harmonic D cyclotron resonance lies in the plasma centre at the same location than the N = 1 H cyclotron resonance (see Fig.8a). This illustrates the delicate interplay between these two auxiliary heating methods.

As briefly mentioned, an important consequence of the low ICRF absorptivity of these heating scenarios is the enhancement of plasma-wall interactions leading to relatively large radiation losses. This is depicted ixn Fig.11 (left), where the total radiated power is shown as function of the ICRF power applied for the N = 1 H (circles) and for the N = 2 ^{3}He (triangles) heating experiments. The data correspond to 0.4s time averaged values sampled throughout the pulses. The density, temperature and NBI power (~1.3MW) were similar in all the time intervals considered.

The fact that the radiation losses for a given ICRF power level are higher for the N = 2 ^{3}He case than for the fundamental H majority case is not only due to the presence of relatively large fractions of ^{3}He in the plasma (higher Z_{eff}), but is also related to a stronger RF-induced plasma-wall interaction observed in the former case, leading to a higher impurity content in the plasma. This is depicted in Fig.11 (right), which shows the line emission intensity of Beryllium (material of the ICRF antenna screen bars) measured by visible spectroscopy as function of the ICRF power for the two scenarios. On this figure one can clearly see a significantly higher Be emission in the N = 2 ^{3}He case. The same time intervals as on the left figure were considered. A similar study for the C^{+6} and C^{+4} spectroscopy measurements (not shown) supported by 2D bolometer tomography indicates that most of the additional radiation observed in the N = 2 ^{3}He case comes from the plasma edge

and the divertor region rather than from the bulk plasma.

Unlike for the non-active operation phase of ITER with ^{4}He plasmas, in which the well established fundamental H minority ICRH scheme can be used (see [34] for its expected performance in ITER), further work is still necessary to identify the most optimal plasma parameters needed to exploit the hydrogen half-field ITER phase to its fullest. Aside from optimizing the above described heating scenarios, one particularly promising heating scheme would be possible for H plasmas. By further reducing the confining magnetic field to 1/3 of its nominal value, the bulk hydrogen plasmas could be heated using 2nd harmonic H ICRF heating. While such reduced field may be too small to ensure good confinement, theoretical predictions suggest that it may be ideal for testing the RF system in ITER. Indeed, the expected single pass absorption for this scenario is nearly 100% with dominant ion heating [35], thanks to the enhancement of N=2 ion-cyclotron absorption with the resonant ion species concentration.

Finally, prior to actually using the fusion fuels D and T, initial exploration of the performance of the ITER machine at full field ($B_0 = 5.3$T) will be done. In that case the ICRF heating schemes rely on heating ^{3}He ions at their fundamental cyclotron resonance layer in either H or ^{4}He plasmas (see Fig8.c). If ^{3}He minority heating in ^{4}He plasmas is a well known and efficient heating scheme [36, 37], ^{3}He heating in H plasmas is a more delicate scenario. For this scheme, referred as *inverted* heating scenario, the charge-to-mass ratio (Z/A) of the minority is smaller than that of the majority and thus the mode conversion layer at the ion-ion hybrid resonance is located at the low field side rather than at the high field side of the minority cyclotron resonance. This scenario was studied a few years ago at very low ^{3}He concentrations [38] and was recently revisited going to higher X[^{3}He] range [39]. Efficient ^{3}He minority heating is achieved only at very low concentrations X[^{3}He]~1-2% (compared to ~7-10% in standard non-inverted scenarios) with the mode conversion regime already reached from ~ 2% (whereas it is typically found around 12-15% in usual mode-conversion heating schemes). Heating efficiencies up to 70% were achieved at X[^{3}He]~1% but the scenario is very sensitive to the gas mixture. Impurities may render it difficult to tune the parameters to ensure optimal heating: earlier as well as recent JET experiments identified the touchiness of the scheme to small amounts of D-like impurities (e.g. C^{+6}) that come from the JET walls and contaminate the plasma. Other impurities such as Be^{+4} may play a similar role in ITER. However, provided the plasma composition can be carefully monitored and controlled, this scheme offers good perspectives for heating the ITER plasmas during its non-active full magnetic field operation phase.

6. SUMMARY AND FUTURE

During recent years, the JET experimental program addressed a number of points that needed to be understood to guarantee successful operation of RF heating in next-step fusion devices such as ITER. Somewhat artificially subdividing the fate of RF power from the generators to the plasma particles into three coupled domains of interest, (1) generator-to-antenna, (2) antenna-to-edge-plasma and (3) edge-to-core-plasma, a series of achievements have been presented in this paper.

(1) POWER EVOLUTION BETWEEN THE GENERATOR AND THE ANTENNA:

Significant amounts of ICRF power (~8MW) have successfully been coupled to ELMy H-mode plasmas relying on optimised matching circuits between the antenna generator and the wave launchers. ELM resilience was demonstrated using both 3dB hybrid couplers and conjugate-T configurations.

ITER-relevant antenna voltages (~45kV) and surface power densities (~6MW/m^2) have been reached with the compact 'ITER-like' antenna without excessive increase of RF sheath effects and RF-induced plasma-wall interaction.

Through combined coarse grain inter-shot analysis and dedicated real-time matching experiments it was demonstrated that compact antenna arrays - although characterized by strong inter-strap cross-talk – can be successfully tuned to couple power to plasmas in a wide range of plasma conditions.

(2) POWER COUPLED FROM THE ANTENNA TO THE PLASMA:

Predictive and interpretative modelling tools were developed to allow further optimization of the design of ICRF antennas. A high degree of confidence in such tools was reached by cross-checking the theoretical calculations with the experimentally obtained values.

Coupling computations done for some JET experiments have demonstrated the huge impact of the uncertainties of the scrape-off layer density profile on the calculations of the coupled power. Although the ICRF power specifications for ITER ($P_{RF} > 20$MW) are still met under the most pessimistic density profiles considered, this is clearly an area to which more attention needs to be devoted in the future as the coupled power can differ up to an order of magnitude depending on the density profile facing the antenna.

To guarantee optimal coupling, optimizing the antenna design is crucial. But since the exact shape and characteristics of the ITER scrape-off layer will not be known until the first plasmas will be created in this machine, exploring methods for shaping the density profile in front of the antenna is a tool that can help ensuring better coupling. Gas puff experiments done in JET and in other machines [23] and only briefly mentioned here, showed promising results. The continuation of these studies planned for the near future should allow getting a firmer grip on the physics involved. There is clear evidence that non-absorbed RF power has a deleterious impact on the release of particles from plasma facing components, in particular in low single pass absorption schemes. Additionally, effects such as RF sheath-induced heat loads, not discussed here, require further attention. With the change of JET's first wall material from C to Be and Tungsten (W) [40], particular attention will be given to this research area with experiments to be conducted in the near future to assess the interaction between ICRF power and such metallic walls.

(3) POWER ABSORPTION INSIDE THE PLASMA:

ICRF heating schemes for ITER's activated phase have already been studied in JET two decades ago (see [41] and references therein). New experiments are planned to take place in the next years

in the presence of the Be wall and W divertor [42]. However, no major obstacles are expected for operating the ICRF system in ITER's activated DT phase.

Both H and ^{4}He are foreseen as the main working gases in ITER's non-activated phase, when the machine will be operated at half its nominal magnetic field ($B_0 = 2.65$T). Heating H ions at their fundamental cyclotron frequency in ^{4}He plasmas is a well established heating scheme and is expected to perform very well in ITER. For H plasmas two heating schemes are available: fundamental majority H and second harmonic ^{3}He ICRF heating. Both these schemes were tested recently in JET, adopting the exact ITER magnetic field, RF working frequency and electron density but evidently operating at lower temperature. While neither of the two is overly promising, they offer sufficient potential for application in ITER within their moderate heating capabilities.

The results from the fundamental H majority ICRF experiments confirmed the low heating efficiency expected from theory (the wave polarization near the minority cyclotron layer prohibits efficient ion absorption). Simplified numerical predictions for ITER's half-field plasma parameters suggest a moderate heating efficiency (~50%) with margin for performance optimization based on the dilution of the H plasmas with another ion species (e.g. ^{4}He) to change the wave polarization or by operation at higher plasma temperatures to broaden the Doppler-shifted ICRF absorption. Second harmonic ^{3}He cyclotron heating equally proved to be of limited potential in JET. Although this heating scheme becomes more efficient at high ^{3}He concentrations, it is characterized by low single pass absorption when typical ^{3}He concentrations expected for ITER are considered. The heating efficiency estimated for ITER is also around 50% but opposite to results of H majority heating scheme, this value is not very sensitive to the bulk plasma temperature.

Experiments on fundamental ICRF heating of ^{3}He minority ions in H plasmas, a heating scheme to be used in the non-active full field operation phase of ITER, have shown that this is a well performing scenario if the ^{3}He concentration is kept below 1-2%. The strong influence of impurities such as C or Be on the heating efficiency and on the transition to the mode-conversion heating regime has been confirmed.

In conclusion it can be stated that significant progress has been made over the last years to make ICRF heating a robust heating scheme for the next-step fusion devices. As well from the antenna tuning, the coupling as the heating point of view, RF heating is getting ready for ITER, with a number of issues - as e.g. a better understanding of the interaction between the RF waves and the plasma edge and first wall - to be further addressed in the coming years.

REFERENCES

[1]. ITER team et al., Nuclear Fusion **39** (12) (1999) p.2137.

[2]. P. Lamalle et al., 18th Topical Conf. on RF Power in Plasmas, AIP Conf. Proc. 1187, 2009, p.265.

[3]. A. Kaye et al., Fusion Engineering and Design **74** (1994) 1-21

[4]. M.-L. Mayoral et al., 17th Topical Conf. on RF Power in Plasmas, AIP Conf. Proc. 933, 2007, p.143.

[5]. J-M. Noterdaeme et al., 13th Topical Conf. on RF power in Plasmas, AIP Conf. Proc. 485, 1999, p.92.
[6]. D. Pozar, "Microwave Engineering (3rd edition)", John Wiley and Sons, USA, 2005.
[7]. I. Monakhov et al., 18th Topical Conf. on RF Power in Plasmas, AIP Conf. Proc. 1187, 2009, p205.
[8]. Mayoral et al., 36th EPS Conference on Plasma Physics, ECA Vol. **33**E, O-4.048 (2009).
[9]. F. Durodie et al., Fusion Engineering and Design **74** (2005) 223-228
[10]. M. Nightingale et al., 18th Topical Conf. on RF Power in Plasmas, AIP Conf. Proc. 1187, 3009, p.213.
[11]. V.P. Bhatnagar et al., Plasma Physics and Controlled Fusion **31** (1989) 2111
[12]. F. Durodie et al., 23rd IAEA Fusion Energy Conference 2010, Daejeon, Korea.
[13]. R. Bilato et al., Nuclear Fusion **45** (2005) L5-L7.
[14]. D. Milanesio and R. Maggiora, Nuclear Fusion **50** (2010) 025007.
[15]. A. Messiaen and R. Weynants, Plasma Physics and Controlled Fusion **53** (2011) 1-29
[16]. A. Messiaen et al., Nuclear Fusion **50** (2010) 1-21.
[17]. E. Lerche et al., 18th Topical Conf. on RF Power in Plasmas, AIP Conf. Proc. 1187, 2009, p.93.
[18]. D. Van Eester et al., Plasma Physics and Controlled Fusion **40** (1998) 1949–1975
[19]. Ph. Jacquet et al., 'Heat-Loads on JET Plasma Facing Components from ICRF and LH Waves', submitted to Nuclear Fusion.
[20]. A. Czarnecka et al., 'Impurity Production by the ICRF Antennas in JET', to appear in special TF-H edition of Plasma Physics and Controlled Fusion.
[21]. F.W. Perkins et al., Nuclear Fusion **29** (4) (1989) p.583-592.
[22]. V. Bobkov et al., 18th Topical Conf. on RF Power in Plasmas, AIP Conf. Proc. 1187, 2009, p125
[23]. M.L. Mayoral et al., 23rd IAEA Fusion Energy Conference 2010, Daejeon, Korea.
[24]. G. Wassenhove et al., 38th EPS Conf. on Plasma Physics, Strasbourg (2011).
[25]. V. Bergeaud et al., Nuclear Fusion **40** (2000) 35.
[26]. D. Van Eester et al., Nuclear Fusion **42** (2002) 310–328.
[27]. F.W. Perkins et al., Nuclear Fusion **17** (1977) p.1197.
[28]. E. Lerche et al., 37th EPS Conf. on Plasma Physics, Dublin (2010), ECA 34A, O4.121
[29]. E. Lerche et al., Plasma Physics and Controlled Fusion **50** (2008) 035003.
[30]. M.G. von Hellermann et al., Review of Scientific Instruments **61** (1990) 3479.
[31]. E. de la Luna et al., Review of Scientific Instruments **75** (2004) 3831.
[32]. D. Van Eester et al., Plasma Physics and Controlled Fusion **51** (2009) 044007
[33]. V. Kiptily et al., 'Fast ions in mode conversion heating (^{3}He)-H plasmas in JET', to appear in special TF-H edition of Plasma Physics and Controlled Fusion.
[34]. E. Lerche et al., 19th Topical Conf. on RF Power in Plasmas, Newport (2011)

[35]. E. Lerche et al., 23rd IAEA Fusion Energy Conference2010, Daejeon, Korea.
[36]. Mantsinen et al. Nuclear Fusion **44** (2004) 33–46.
[37]. Mantsinen et al., Physical Review Letters **89** (11) 2002.
[38]. M.-L. Mayoral et al., Nuclear Fusion **46** (2006) S-550–S-563
[39]. D. Van Eester et al., "Heating (^{3}He)-H JET plasmas with multiple mode conversion layers", to appear in special TF-H edition of Plasma Physics and Controlled Fusion.
[40]. R. Neu et al., 38th EPS Conf. on Plasma Physics, Strasbourg (2011).
[41]. D. Start et al., Nuclear Fusion **39** (1999) p.321
[42]. A.C.C. Sips et al., 38th EPS Conf. on Plasma Physics, Strasbourg (2011).

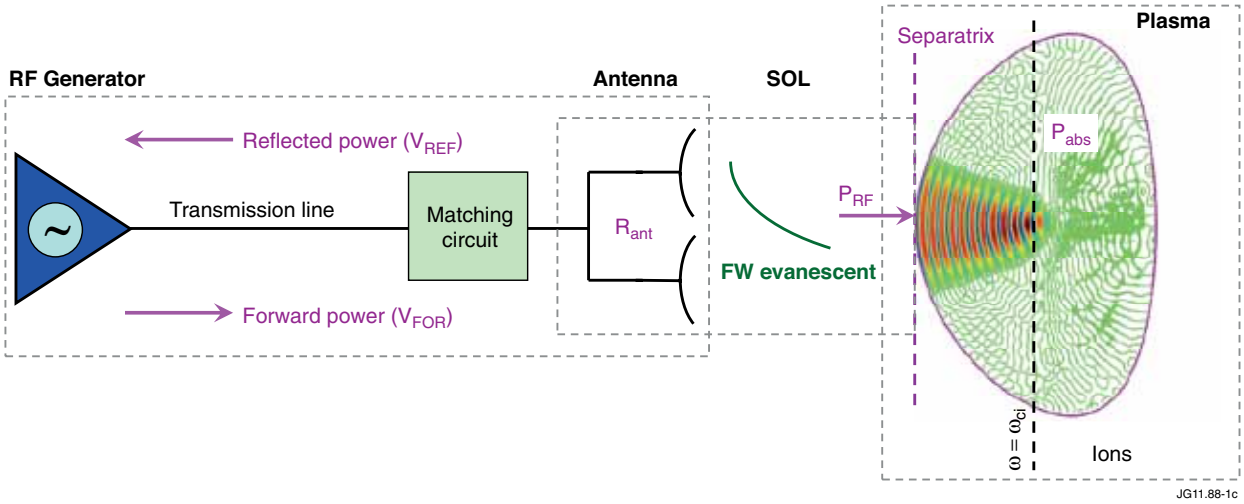

Figure 1: Chart illustrating the principle of the ICRF heating process.

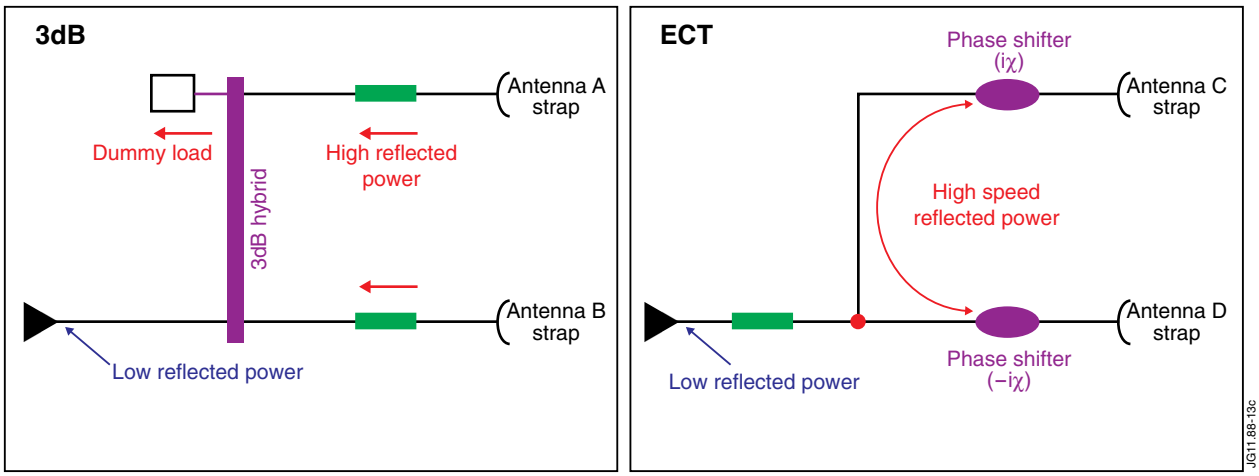

Figure 2: Load resilient circuit layouts of the A2 antennas: (left) The 3dB hybrid concept used in the antenna modules A and B; (right) The (External) Conjugate-T configuration (ECT) used to operate antennas C and D in ELM resilient mode.

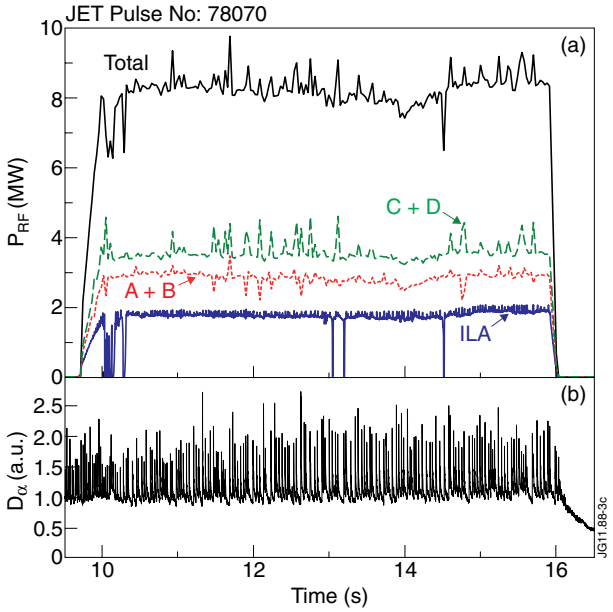

Figure 3: ELM resilient operation of the ICRF system in JET: (a) ICRF power coupled by antennas A+B (dotted), antennas C+D (dashed) and by the ILA (solid); (b) D_α- emission illustrating the strong type-I ELM's in the discharge.

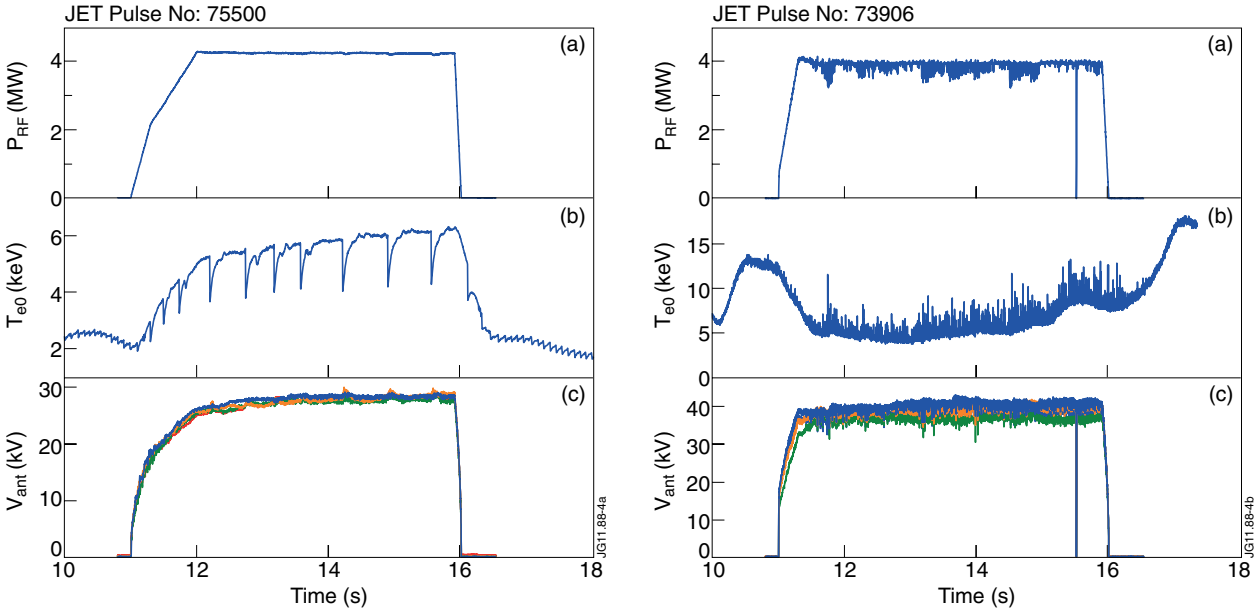

Figure 4: (left) High power density ILA pulse (L-mode): (a) ICRF power, (b) central electron temperature, (c) voltage on four antenna straps; (right) High antenna voltage ILA pulse (H-mode): (a) ICRF power, (b) D_α emission, (c) voltage on four antenna straps;

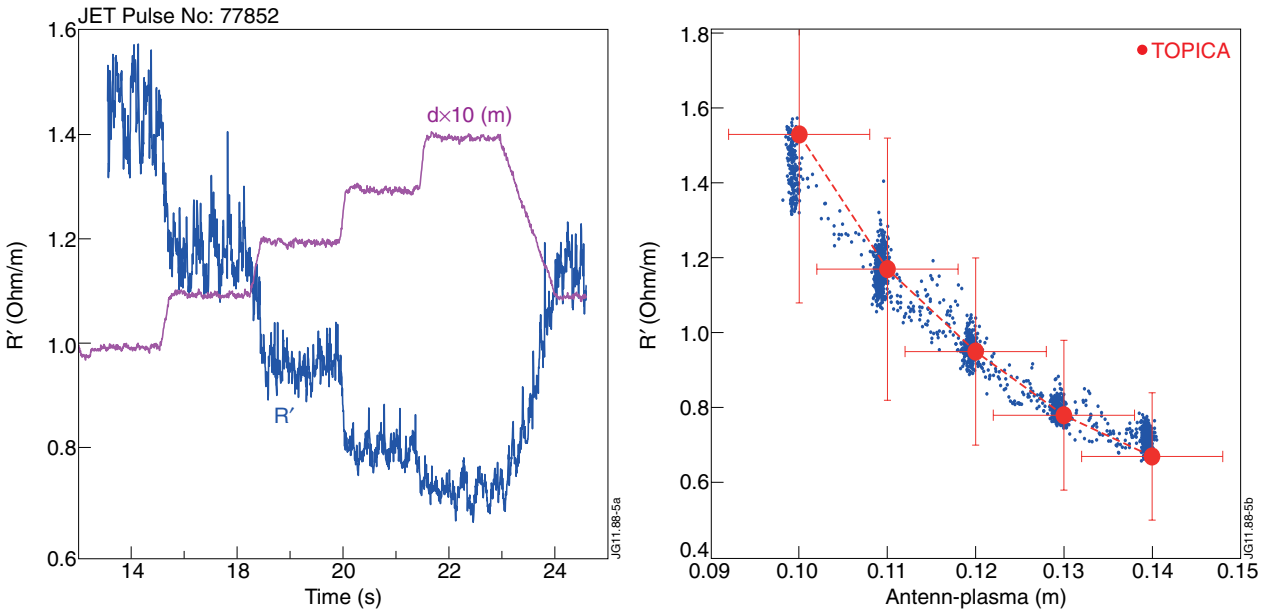

Figure 5: (left) Time traces of the coupling resistance of one pair of the ILA straps together with the antenna-plasma distance (x10) in L-mode Pulse No: 77852 at f = 42MHz; (right) Coupling resistance versus antenna-plasma distance for the same discharge together with the numerical modelling done with the TOPICA code.

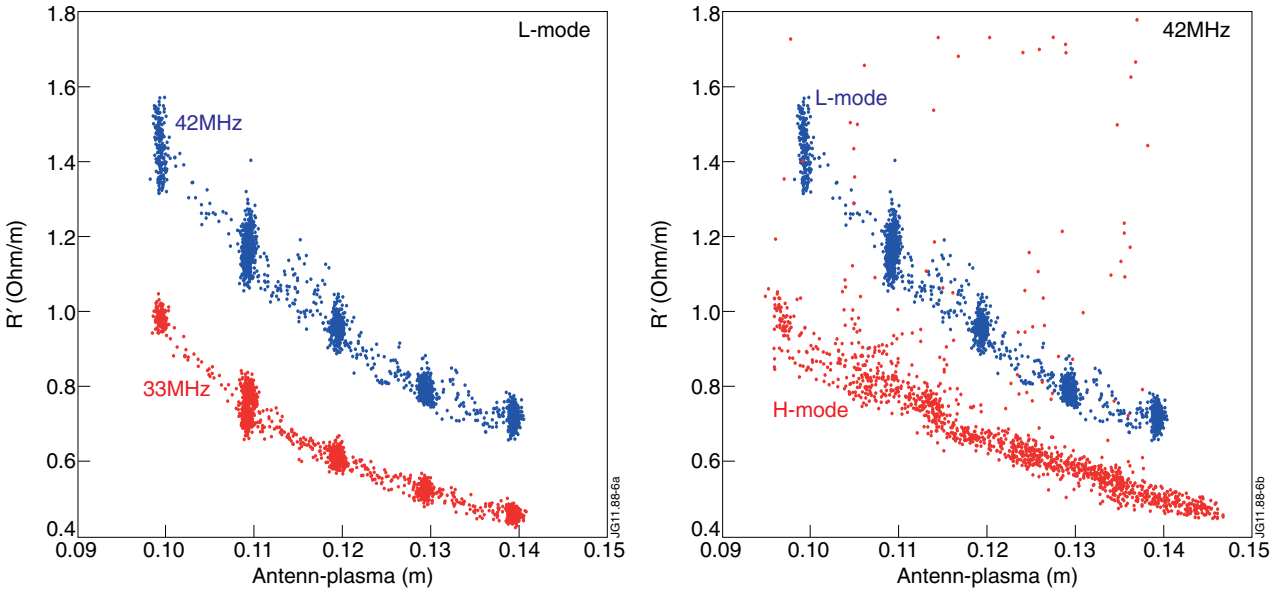

Figure 6: Comparison of the coupling resistance obtained in the reference Pulse No: 77852 (L-mode, 42MHz) with a similar discharge with the RF operating frequency reduced to f = 33MHz (JET Pulse No: 77847); (right) Comparison of the reference pulse with a discharge with same operating frequency but in H-mode (JET Pulse No: 77851), where steeper density gradients are present in the plasma edge.

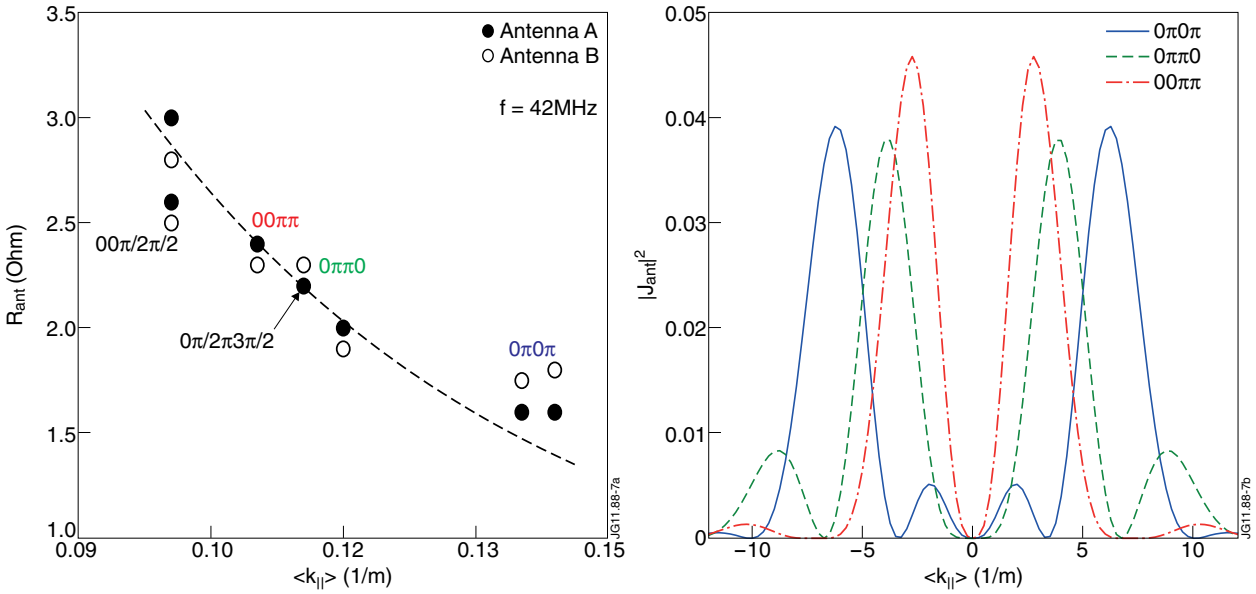

Figure 7: (left) Coupling resistance of the A2 antennas as function of the dominant $k_{//}$ wavenumber excited in different phasing configurations (JET Pulse No: 74091-74094, 78727-78732); (right) Example of the $k_{//}$-spectra excited by the A2 antennas computed with the ANTITER II code for 3 cases: 0π0π (solid), 0ππ0 (dashed) and 00ππ (dash-dotted).

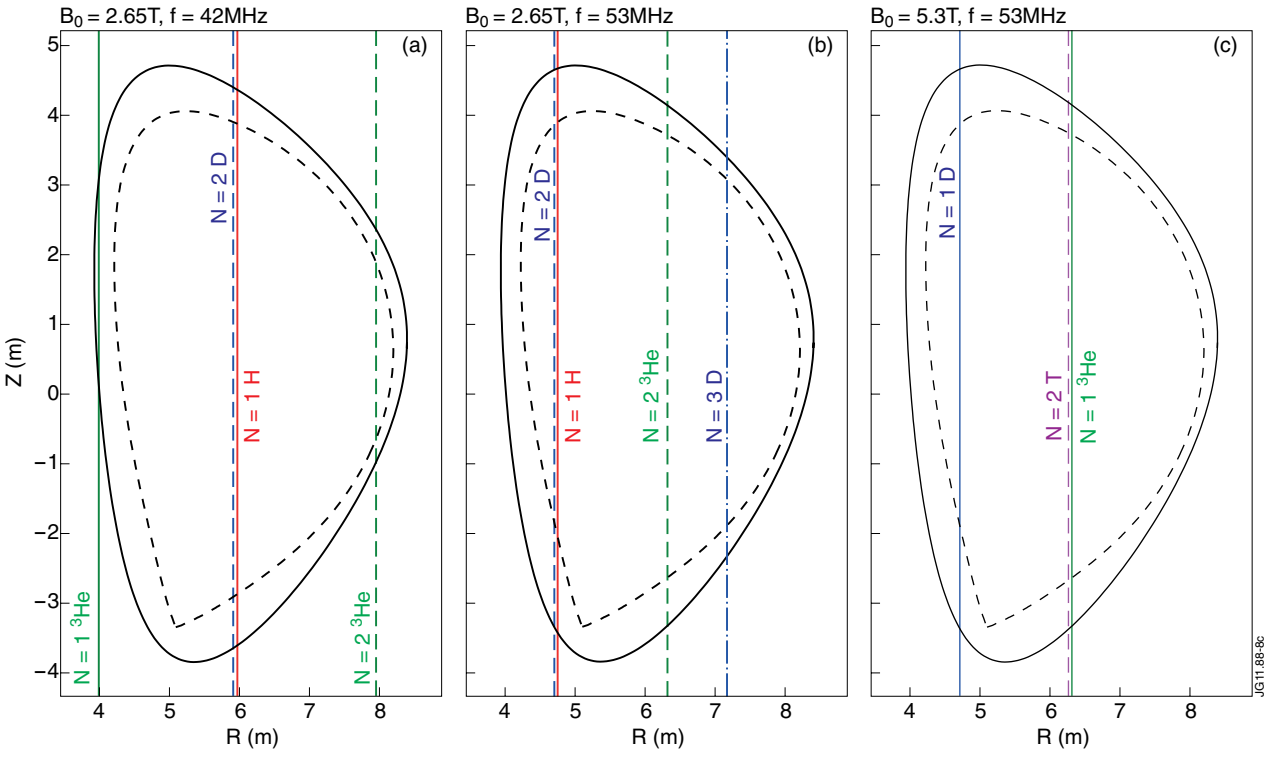

Figure 8: Location of the main fundamental (solid), 2nd harmonic (dashed) and 3rd harmonic (dash-dot) ion cyclotron resonances of various ion species in different conditions for ITER: (a) $B_0 = 2.65T$ and $f = 42MHz$; (b) $B_0 = 2.65T$ and $f = 53MHz$; (c) full-field DT operation at $B_0 = 5.3T$ and $f = 53MHz$.

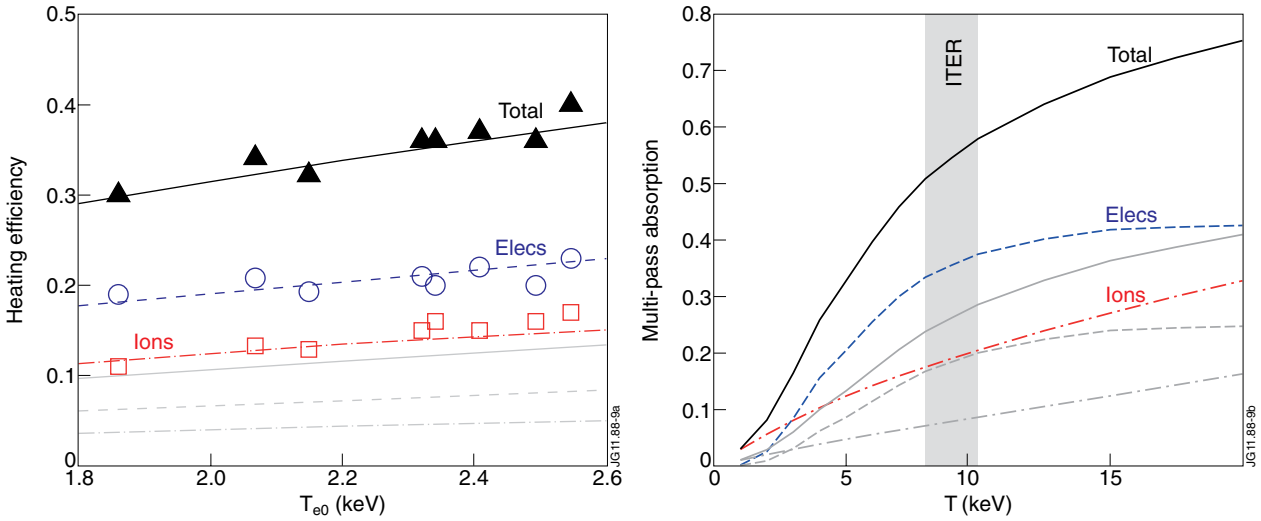

Figure 9: (left) Experimental heating efficiencies (ions = squares, electrons = circles, total = triangles) obtained in the H majority heating experiments in JET (JET Pulse No: 79330-79335) as function of the plasma temperature together with the multi-pass absorption predictions (ions = dash-dotted, electrons = dashed, total = solid) based on the single pass absorption values computed with the TOMCAT code (light grey curves) by considering 22% of power losses per wave pass in the plasma; (right) Multi-pass absorption (ions = dash-dotted, electrons = dashed, total = solid) estimated from the TOMCAT results for ITER's half-field plasma conditions adopting the same losses as found from the JET experiments (again, the grey curves indicate the single pass absorption values used in the multi-pass model).

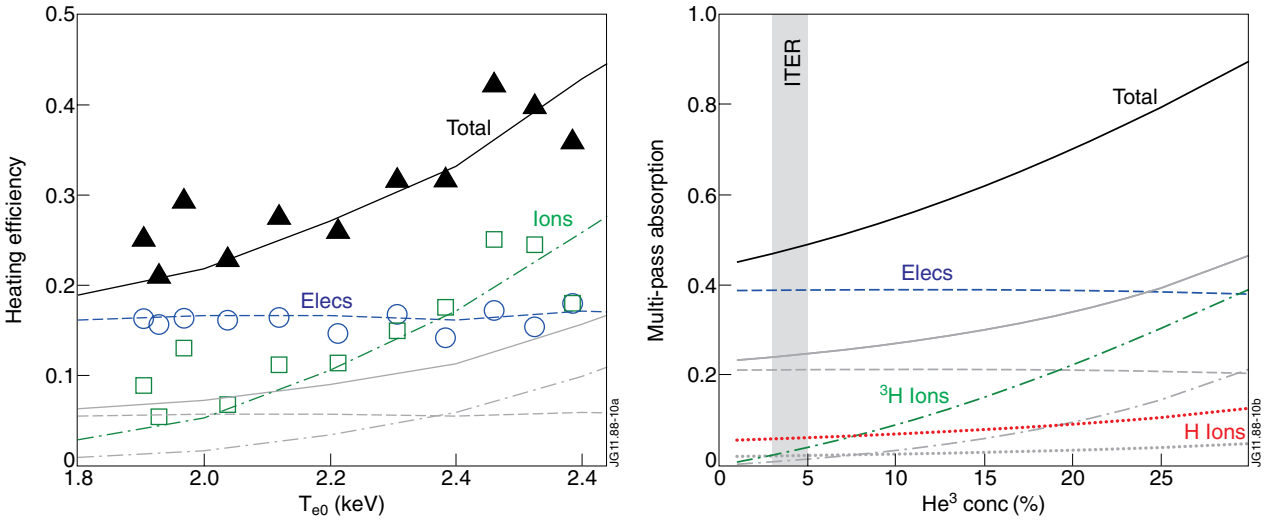

Figure 10: (left) Experimental heating efficiencies (ions = squares, electrons = circles, total = triangles) obtained in the N = 2 ^{3}He heating experiments in JET (JET Pulse No: 79352) as function of the ^{3}He concentration together with the multi-pass absorption predictions (ions = dash-dotted, electrons = dashed, total = solid) based on the single pass absorption values computed with the TOMCAT code (grey curves) considering 26% of power losses per wave pass in the plasma; (right) Multi-pass absorption (ions = dash-dotted, electrons = dashed, total = solid) estimated from the TOMCAT results for ITER's half-field plasma conditions adopting the same losses as found from the JET experiments (the grey curves indicate the single pass absorption values used in the multi-pass model).

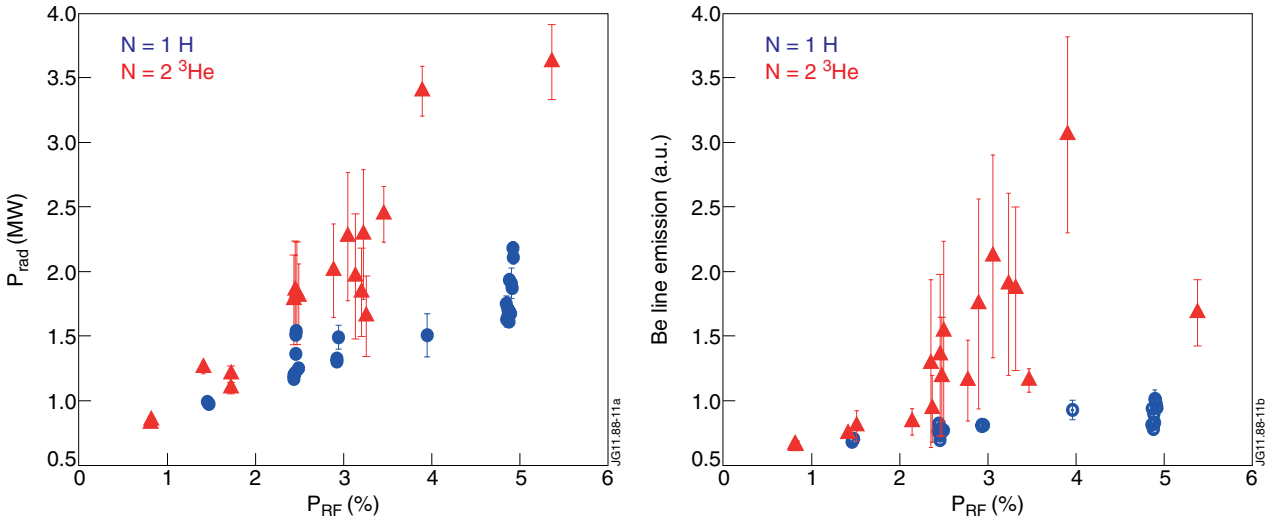

Figure 11: Total radiated power (left) and intensity of Be line (right) as function of the ICRF power in a series of discharges of the N = 1 H majority (circles) and the N = 2 ^{3}He (triangles) ICRF heating experiments (JET Pulse No: 79330-79335, JET Pulse No: 79343-79352).